energy&fuels

Article

pubs.acs.org/EF

Simulation and Multi-Objective Optimization of a Trickle-Bed Reactor for Diesel Hydrotreating by a Heterogeneous Model Using Non-Dominated Sorting Genetic Algorithm II

Ali Bakhshi Ani, Habib Ale Ebrahim,* and Mohammad Javad Azarhoosh

Chemical Engineering Department, Petrochemical Center of Excellence, Amirkabir University of Technology, Tehran 15875-4413, Iran

ABSTRACT: Hydrotreating processes for diesel fuels are becoming increasingly important, owing to environmental regulations limiting sulfur and aromatic compounds, which are becoming more strict. Among investigations into hydrotreating modeling, most of the studies use a homogeneous model to simulate the reactor. However, for a real industrial reactor, that is not always an accurate assumption. Furthermore, reports of efforts to find the best operating conditions are very scarce. In this study, a heterogeneous model of three main reactions—hydro-desulfurization, hydro-denitrogenation, and hydro-dearomatization—was applied to simulate the hydrotreating reactor. The model results show a good agreement with literature experimental data. The effects of important operational parameters such as temperature, pressure, liquid hourly space velocity, and H_2/oil ratio on various hydrotreating reactions are also evaluated. Finally, a multi-objective optimization based on non-dominated sorting genetic algorithm II is carried out to find the best operating conditions for a diesel fuel hydrotreating reactor.

1. INTRODUCTION

1.1. Hydrotreating Process. Hydrotreating (HT) processes for diesel fuels are becoming increasingly important, owing to environmental regulations limiting sulfur and aromatic compounds, which are becoming more strict. For example, in 2009, the European Union restricted the total sulfur content of gasoline and diesel to 10% wppm.[1] Furthermore, HT processing protects catalysts and equipment in down-stream processes from poisoning and corrosion by sulfur components.

Now that hydrogen can be produced at low cost and in large scale from steam reforming, HT processes have developed rapidly. Various HT processes are used to eliminate contaminants such as sulfur, nitrogen, and olefins, and to reduce aromatics, from oil fractions, and petroleum products are stabilized by reacting them with hydrogen.[2]

In HT processes, the hydro-desulfurization (HDS), hydro-denitrogenation (HDN), and hydro-dearomatization (HDA) reactions are done in a trickle-bed reactor (TBR), in which three phases—gas, liquid, and solid—exist together and come into contact. These phases are rich hydrogen gas, oil fraction liquid, and solid catalysts.

The feeds of HT processes include a wide range of feedstocks, from naphtha to residues. In HT of diesel, the goals are to eliminate sulfur compounds (for environmental considerations) and to reduce aromatics (for enhancing cetane number). The conventional HT catalysts are sulfides of cobalt and molybdenum on alumina support. However, when the aim is to remove nitrogen components, nickel–molybdenum on alumina is more effective.[3]

1.2. Hydrotreating Modeling. Fixed-bed reactors, in particular TBRs, can be modeled by a variety of approaches based on hydrodynamics, continuous models, and empirical correlations. Among studies in the literature, the continuous model has been widely used due to its reliability. Some advantages this approach offers are the following:[4]

- It is appropriate for scale-up and scale-down.
- It is suitable for kinetic studies.
- The internal diffusion through particles can be considered.

The most popular classification in the continuous model is heterogeneous vs homogeneous models. The heterogeneous model considers the internal gradient of the concentration through the catalyst pellets, while the homogeneous model assumes the fluid–particle system to be a single phase and neglects the effect of internal resistance of the catalyst pellets in the process.[4]

Korsten and Hoffmann may have been the first scientists to model the HT process.[5] Their model was based on two-film theory and included mass-transfer coefficients, solubility data, and properties of compounds, and they considered only the HDS reaction in the reactor. Their model showed a good agreement with experimental data. They found that the gas/oil flow ratio in the reactor had a significant effect on the sulfur content in the product.

The paper by Bhaskar and co-authors is more complete, in that they considered HDS, HDN, and HDA in modeling of TBR for the diesel HT process.[6]

An experimental plug-flow TBR for HDS has been modeled by Mejdell and co-workers.[7] Their model was based on a discretization of sulfur components into small pseudo-components, and they used the Langmuir–Hinshelwood kinetic expression. They carried out experiments on a laboratory reactor to find the kinetic parameters.

Lopez and Dassori developed a one-dimensional heterogeneous model for simulation of a commercial TBR and evaluated the effect of important operating parameters.[8] They

Received: March 4, 2015
Revised: April 20, 2015
Published: April 20, 2015

DOI: 10.1021/acs.energyfuels.5b00467
Energy Fuels 2015, 29, 3041−3051

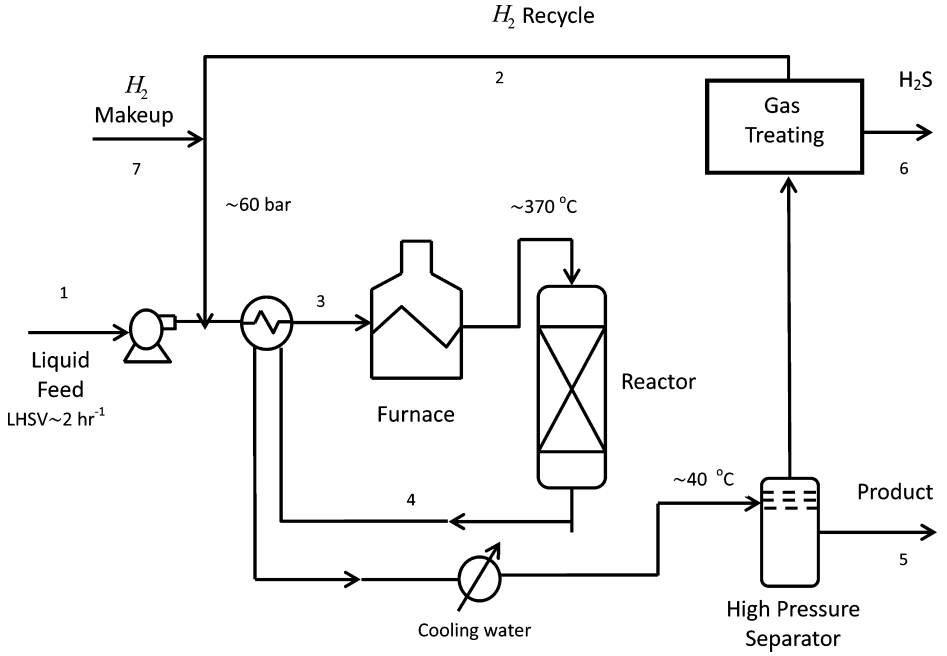

Figure 1. Simple schematic diagram of the hydrotreating process.

considered HDS and HDN reactions and assumed that the gas and the liquid phases were plug-flow. In addition, their model took into account the catalyst deactivation caused by metal deposition and coking.

Avraam and Vasalos developed a steady-state model for TBR and considered a plug-flow fixed-bed reactor with axial dispersion.[9] They found that as the inlet temperature increased, the removal of sulfur components also increased.

Rodriguez and Ancheyta studied the HDS, HDN, and HDA reactions in a vacuum gas oil (VGO) hydrotreater.[10] They modeled the reactor on the basis of two-film theory, and the HDS reaction was described by Langmuir−Hinshelwood kinetics. The HDN was modeled in two steps, in which nonbasic compounds are first hydrogenated to basic nitrogen compounds, which then undergo further reaction to remove the nitrogen atom from the molecule. The HDA was presented as a first-order reversible reaction. They validated the model on the basis of experimental data which were obtained from a pilot plant and studied the effects of temperature and space velocity on the performance of the HT reactions.

Jimenz and co-authors modeled an industrial VGO HT reactor and considered simultaneous reaction for HDS, HDN, HDA, along with the inhibition effects among different molecules.[11] They mentioned that with increasing temperature, the HDS and HDN reactions improved. The conversion increased for poly-aromatics as the temperature was increased until 370 °C, and after that temperature it was reduced due to the reversibility of the reaction.

Melis and co-workers used a homogeneous axial dispersion model. Their model considered only the HDA reaction in gas oil and was able to make predictions about different types of feed with different concentrations of aromatics very well.[12]

Macias and Ancheyta studied the effects of different catalyst shapes on the characteristics and behavior of a HDS catalyst and reactor, such as concentration gradients, sulfur content in the product, and pressure drop.[13]

The effect of co-current and counter-current flows in TBRs on removal of sulfur was investigated by Cheng and co-workers.[14] They used a one-dimensional heterogeneous model with HDS and HDA reactions. Their results showed that the reactor performed better in counter-current mode.

Mederos and co-workers carried out a dynamic modeling for HT of diesel obtained from heavy crude oil.[15] They evaluated the effects of changing concentration, partial pressure, and temperature on the dynamic behavior of the system.

Jarullah and co-workers proposed a kinetic model for hydrodeasphaltenization in a TBR for improving fuel quality by whole crude oil HT.[16] In their work, first the unknown parameters for the reaction were obtained by a series of experiments, and then the model and the estimated kinetic parameters were applied to simulate the reactor in different operating conditions.

1.3. Process Description. Figure 1 shows a simple flow diagram of the HT process. In this figure, stream 1 contains liquid oil feed which is mixed with recycled hydrogen (stream 2) and makeup hydrogen (stream 7). This mixture (stream 3) is preheated with the outlet stream from the reactor (stream 4) and is fed to the heater to reach to the proper temperature (about 370 °C) for inlet to the reactor. Next, the mixture enters from the top of a fixed-bed reactor, and hydrogen reacts with the oil in the presence of HT catalyst to produce hydrogen sulfide, ammonia, and saturated hydrocarbons. The effluent (stream 4) is cooled to about 40 °C, and hydrogen-rich gas is isolated using a high-pressure separator. This gas is treated to remove hydrogen sulfide (stream 6), and then hydrogen is compressed to about 60 bar and recycled to the reactor after mixing with makeup hydrogen. Finally, the hydrotreated diesel (stream 5) is produced.[2] Typical operating conditions for the process are also shown in Figure 1.

1.4. Goals of This Study. Among reported investigations in HT modeling, most of the studies used a homogeneous model to simulate the reactor. However, for a real industrial reactor, this is not always an accurate assumption. Furthermore, reports of efforts to find the best operating conditions are very scarce. Therefore, the aim of this work is to apply a heterogeneous model to simulate the HT reactor. The effects of important

DOI: 10.1021/acs.energyfuels.5b00467
Energy Fuels 2015, 29, 3041−3051

operational parameters such as temperature, pressure, liquid hourly space velocity (LHSV), and H_2/oil ratio on HDS, HDN, and HDA reactions will then be evaluated. Finally, a multi-objective optimization based on non-dominated sorting genetic algorithm II (NSGA II) is carried out to find the best operating conditions for the diesel HT reactor.

2. KINETICS AND REACTOR MODELING

2.1. Reaction Kinetics Model. The kinetics of HDS reaction is described by Langmuir–Hinshelwood relation as follows:[17]

Table 1. Kinetic Parameters for HDS, HDN, and HDA Reactions[17,18]

reaction	E_a (kJ/mol)	k_0
HDS	131.99	4.266×10^9 cm^3 g^{-1} s^{-1} cm^3 mol$^{-0.45}$
HDN_{NB}	164.94	3.62×10^6 s^{-1} (wt%)$^{-0.5}$
HDN_B	204.34	3.66×10^{11} s^{-1} (wt%)$^{-0.5}$
HDA		
forward	80.1	231.945 s^{-1} MPa^{-1}
reverse	112.6	1.266×10^5 s^{-1}

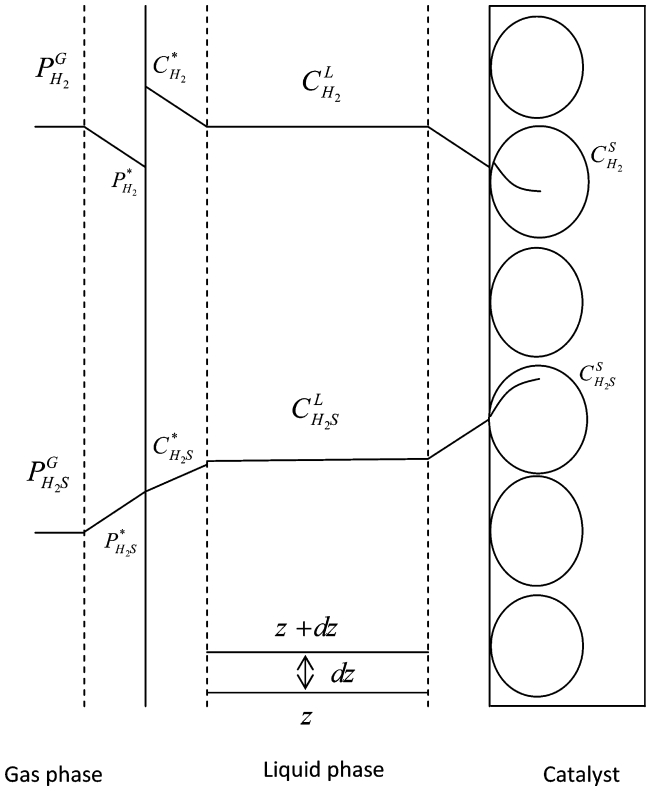

Figure 2. Schematic of application of two-film theory for heterogeneous trickle-bed reactor.

$$r_{HDS} = k_{HDS}\frac{C^s_S(C^s_{H_2})^{0.45}}{(1 + K^s_{H_2}C^s_{H_2S})^2} \quad (1)$$

In HDN, non-basic nitrogen (N_{NB}) converted first to basic nitrogen (N_B), which undergoes further reaction to eliminate the nitrogen from the molecule. Thus, the following kinetic expressions are considered for HDN:[17]

$$r_{HDN_B} = k_{N_{NB}}(C_{N_{NB}})^{1.5} - K_{N_N}(C_{N_N})^{1.5} \quad (2)$$

$$r_{HDN_{NB}} = k_{N_{NB}}(C_{N_{NB}})^{1.5} \quad (3)$$

The HDA was represented by a reversible reaction as follows:[18]

$$r_{HDA} = k_f p_{H_2} C_A - k_r C_N \quad (4)$$

Kinetic parameters of HDS, HDN, and HDA reactions are given in Table 1.

2.2. Reactor Model. The HT reactor was modeled on the basis of two-film theory.[5] Figure 2 displays a schematic of application of this theory and heterogeneous system for a TBR.

The mass-balance equation for components in the gas phase in the reactor is[5]

$$\frac{u_G}{RT}\frac{dp^G_i}{dz} + k^G_i a_L\left(\frac{p^G_i}{H_i} - C^L_i\right) = 0 \quad (5)$$

where u_G is the superficial gas velocity, R is the universal gas constant, T is absolute temperature, p^G_i is the partial pressure of gaseous i, z is the length of the reactor, $k^G_i a_L$ is the gas–liquid mass-transfer coefficient, H_i is the Henry's law coefficient, and C^L_i is the concentration in the liquid phase, with $i = H_2$ or H_2S.

The mass-balance equation for gaseous components in liquid phase is[5]

$$u_L\frac{dC^L_i}{dz} - k^L_i a_L\left(\frac{p^G_i}{H_i} - C^L_i\right) + k^s_i a_s(C^L_i - C^s_i) = 0 \quad (6)$$

where u_L is the superficial liquid velocity, C^L_i and C^s_i are the concentrations in liquid and surface of the catalyst, z is the length of the reactor, $k^G_i a_L$ and $k^s_i a_s$ are the gas–liquid and liquid–solid mass-transfer coefficients, and $i = H_2$ or H_2S.

For liquid components the mass-balance equation is expressed as[5]

$$u_L\frac{dC^L_i}{dz} + k^s_i a_s(C^L_i - C^s_i) = 0 \quad (7)$$

where i = S, N_B, N_{NB}, or A (aromatics).

The mass-balance equation at surface of the catalyst is[5]

$$k^s_i a_s(C^L_i - C^s_i) = -\rho_B \eta_j r_j \quad (8)$$

where ρ_B is the bulk density of the catalyst, η_j is the effectiveness factor for reaction j, r_j is the reaction rate based on catalyst surface concentrations, j = HDS, HDN, or HDA, and $i = H_2$, H_2S, S, N_B, N_{NB}, or A.

The effectiveness factor can be obtained from the following expression:[19]

$$\eta_j = \frac{-r_{j,act}}{-r_{j,surface}} = \frac{3}{R^3_p}\frac{\int r^2(-r_j)\,dr}{-r_{j,surface}} \quad (9)$$

where R_p is the radius of catalyst pellet, $-r_{j,act}$ is the actual rate of reaction, and $-r_{j,surface}$ is the rate of reaction based on the pellet surface conditions. To find $-r_{j,act}$, we need to solve the mass-balance equation in the interior of the catalyst and find the concentrations of reactants inside the pellet.

The mass-balance equation for the catalyst pellet is[20]

$$\frac{d^2C_i}{dr^2} + \frac{2}{r}\left(\frac{dC_i}{dr}\right) - r_j = 0 \quad (10)$$

DOI: 10.1021/acs.energyfuels.5b00467
Energy Fuels 2015, 29, 3041−3051

Table 2. Correlations To Estimate the Properties of Feedstock, Gas Solubilities, and Mass-Transfer Coefficients[5]

parameter	correlation
oil density	$\rho(p, T) = \rho_0 + \Delta\rho_p - \Delta\rho_T$
	$\Delta\rho_p = [0.167 + (16.181 \times 10^{-0.0425\rho_0})]\left(\frac{p}{1000}\right) - 0.01[0.299 + (263 \times 10^{-0.0603\rho_0})]\left(\frac{p}{1000}\right)^2$
	$\Delta\rho_T = [0.0133 + 152.4(\rho_0 + \Delta\rho_p)^{-2.45}](T - 520) - [8.1 \times 10^{-6} - 0.0622 \times 10^{-0.764(\rho_0 + \Delta\rho_p)}](T - 520)^2$
Henry coefficient	$H_i = \frac{\nu_N}{\lambda_i \rho_L}$
solubility of H_2	$\lambda_{H_2} = -0.559729 - (0.42947 \times 10^{-3})T + 3.07539\left(\frac{T}{\rho_{20}}\right) + (1.94593 \times 10^{-6})T^2 + \frac{0.835783}{\rho_{20}^2}$
solubility of H_2S	$\lambda_{H_2S} = \exp(3.3670 - 0.008470T)$
gas–liquid mass-transfer coefficient	$\frac{k_i^L a_L}{D_i^L} = 7\left(\frac{G_L}{\mu_L}\right)^{0.4}\left(\frac{\mu_L}{\rho_L D_i^L}\right)^{1/2}$
dynamic liquid viscosity	$\mu_L = (3.141 \times 10^{10})(T - 460)^{-3.444}[\log_{10}(\mathrm{API})]^a$
	$a = 10.313[\log_{10}(T - 460)] - 36.447$
diffusivity	$D_i^L = (8.93 \times 10^{-8})\left(\frac{\nu_L^{0.267}}{v_i^{0.433}}\right)\left(\frac{T}{\mu_L}\right)$
molar volume	$\nu = 0.285 v_c^{1.048}$
	$v_c^m = (7.5214 \times 10^{-3})(T_{\mathrm{MeABP}}^{0.2896})(d_{15.6}^{-0.7666})$
liquid–solid mass-transfer coefficient	$\frac{k_i^s}{D_i^L a_s} = 1.8\left(\frac{G_L}{a_s \mu_L}\right)^{1/2}\left(\frac{\mu_L}{\rho_L D_i^L}\right)^{1/3}$
specific surface area	$a_s = \frac{6}{d_p}(1 - \varepsilon)$

where r is the radius of catalyst, C_i is the concentration inside the catalyst, and $i = H_2$, H_2S, S, N_B, N_{NB}, or A.

2.3. Property Prediction. The model needs trustworthy correlations to predict the mass-transfer coefficients for gas–liquid and liquid–solid interfaces, gas solubilities, and specification of product and feedstock. These correlations were adapted from the literature and are summarized in Table 2.

3. OPTIMIZATION

3.1. Genetic Algorithm (GA). GA is an optimization tool based on Darwinian evolution. GAs start with randomly chosen parent chromosomes from the search space to create a population. They work with the chromosome genotype. The population evolves toward better chromosomes by applying genetic operators which model genetic processes occurring in the natural selection, recombination, and mutation. Selection compares chromosomes in the population and chooses them to take part in the reproduction process. Selection also occurs with the given probability on the basis of fitness functions, which play the role of an environment for making a distinction between good and bad solutions. The recombination is carried out after finishing the selection process. It combines features of two selected parent chromosomes (with predefined probability) and forms similar children. After the recombination, the offspring undergo mutation. Generally, mutation refers to the creation of a new chromosome from one and only one individual with the predefined probability. After three operations are carried out, the offspring are inserted in the population, replacing the parent chromosomes from which they have been derived and producing a new generation. This cycle is performed until the optimization criteria are met.[21,22]

3.2. Non-dominated Sorting Genetic Algorithm II (NSGA II). The principles on which the NSGA II relies are the same as those of the single-objective optimization. The strongest individuals (or chromosomes) are combined to create the offspring by crossover and mutation, and this scheme is repeated over many generations. However, the multi-objective optimization algorithm must consider the fact that there are many "best solutions" which modify the selection process. NSGA II sorts individuals on the basis of the non-domination rank and the crowding distance to ensure a high level of performance as well as good dispersion of results.[23] In this study, the heterogeneous model was used as an evaluation tool inside the NSGA II.[24] The flowchart of the hybrid of NSGA II based on the heterogeneous model program is shown in Figure 3.

DOI: 10.1021/acs.energyfuels.5b00467
Energy Fuels 2015, 29, 3041−3051

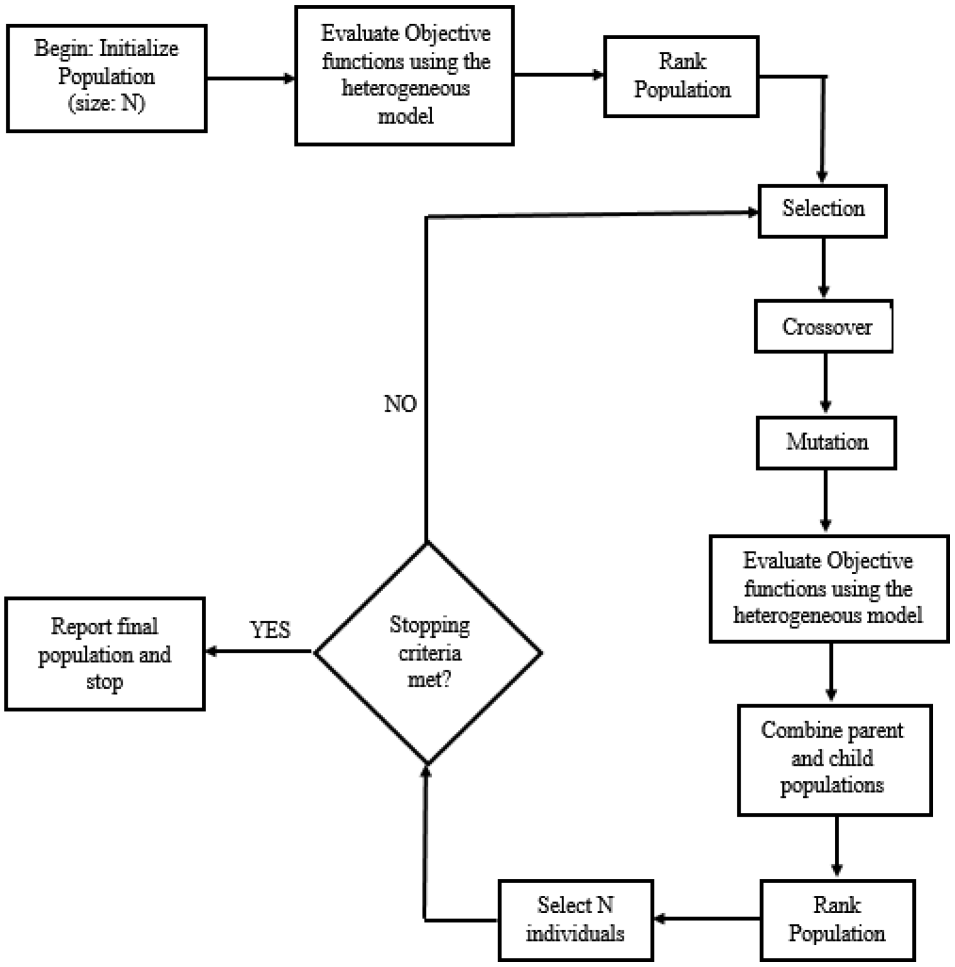

Figure 3. Flowchart of the hybrid of non-dominated sorting genetic algorithm II based on the heterogeneous model program.

4. RESULTS AND DISCUSSION

4.1. Numerical Solution. To solve differential equations, it is necessary to explain the boundary conditions as follows:

(i) Reactor:

$$\begin{aligned}
&\text{at } z = 0, \quad p_{H_2}^G = (p_{H_2}^G)_0 \\
&\qquad p_i^G = 0, \qquad i = H_2S \\
&\qquad C_i^L = (C_i^L)_0, \quad i = H_2,\ S,\ N_B,\ N_{NB},\ \text{and A} \\
&\qquad C_i^L = 0, \qquad i = H_2S \\
&\qquad C_i^S = 0, \qquad i = H_2,\ H_2S,\ S,\ N_B,\ N_{NB},\ \text{and A} \\
&\qquad T = T_0
\end{aligned} \tag{11}$$

(ii) Catalyst pellet:

$$\begin{aligned}
&\text{at } r = 0, \quad \frac{dC_i^s}{dr} = 0 \\
&\text{at } r = R_p, \quad C_i^s = C_i^L, \quad i = H_2,\ H_2S,\ S,\ N_B,\ N_{NB},\ \text{and A}
\end{aligned} \tag{12}$$

The model contains a set of ordinary differential equations along the reactor, and boundary value problem equations for the catalyst pellet coordinate. The ordinary differential equations are solved by using the Runge−Kutta method.[25] The boundary value problem equations are solved using shooting method.[25]

4.2. Model Validation. To validate the model, reported pilot-plant data from the literature were used.[17] Typical feed properties, catalyst specifications, reactor dimensions, and operating conditions are given in Table 3. In the literature experiments, a NiMo sulfide commercial catalyst was used in all tests, and it was diluted with SiC in the reactor.[17] The operating conditions were 380 °C and 5.3 MPa. The reactor temperature was controlled by a three-zone electric furnace, which provided an isothermal temperature for the reaction.

Figure 4 shows a comparison between the predicted and experimental molar concentrations for sulfur, basic nitrogen, non-basic nitrogen, and aromatics along the HT reactor. In addition, the error between predicted and experimental molar concentrations is shown in Table 4. The figure and table show a good agreement with the experimental pilot-plant data, which confirms the ability of the simulation model to predict the concentration of these components in the reactor very well. Furthermore, the concentration of components on a solid surface catalyst is shown in these figures. The concentration reduces from bulk liquid to catalyst surface due to the mass-transfer resistance.

DOI: 10.1021/acs.energyfuels.5b00467
Energy Fuels 2015, 29, 3041−3051

Table 3. Typical Feed and Catalyst Properties and Literature Pilot-Plant Operating Conditions[17]

property	value
Feed	
API	22
molecular weight	441.9
T_{MeABP} (°C)	476
sulfur (wt%)	2.009
total nitrogen (wppm)	1284
basic nitrogen (wppm)	518
total aromatics (wt %)	41.9
Catalyst	
equivalent diameter (mm)	2.54
specific surface area (m^2/g)	175
pore volume (cm^3/g)	0.56
mean pore diameter (Å)	127
molybdenum content (wt%)	10.7
nickel content (wt %)	2.9
bulk density (g/cm^3)	0.8163
Operating Conditions	
temperature (°C)	380
pressure (MPa)	5.3
u_G ($cm\ s^{-1}$)	0.28
u_L ($cm\ s^{-1}$)	1.75×10^{-2}
reactor length (cm)	31.54
LHSV (h^{-1})	2
H_2/oil (std $m^3\ m^{-3}$)	356

Table 4. Error between Predicted and Experimental Molar Concentration Values[10,17]

	molar concn (mol cm^{-3})		
component	expt	pred	error (%)
sulfur	10^{-5}	1.03×10^{-5}	3
non-basic nitrogen	1.302×10^{-6}	1.3027×10^{-6}	0.05
basic nitrogen	6.2×10^{-7}	6.282×10^{-7}	1.32
aromatics	6.5×10^{-4}	6.51×10^{-4}	0.15

Table 5. Input Parameters of NSGA II

no. of decision variables	5
no. of objectives	2
population size	50
crossover method	arithmetic crossover
crossover probability	0.7
mutation method	Gauss method
mutation probability	0.05

4.3. Effect of Operating Conditions. *4.3.1. Effect of Temperature.* The effect of temperature on sulfur and aromatics concentration profiles is shown in Figure 5. The effect of temperature on basic and non-basic nitrogen profiles is similar to the effect on sulfur. The outlet concentrations of sulfur and nitrogen are reduced by raising the temperature, due to the increasing rate of these reactions. But for HDA, the outlet concentration reduces until 360 °C, and above this temperature, the concentration increases due to the reversibility of this saturation reaction.

4.3.2. Effect of Pressure. Figure 6 displays the effect of pressure on the outlet concentrations of sulfur and aromatics. The pressure has no effect on HDN because their reaction rates have no dependence on pressure. Increasing pressure reduces the outlet concentrations of sulfur and aromatics because the rates of these reactions are direct functions of pressure.

4.3.3. Effect of Liquid Hourly Space Velocity (LHSV) and H_2/Oil Ratio. The LHSV is defined as the ratio of feed flow rate to volume of the catalyst.[2] The effect of LHSV on outlet concentrations of sulfur and aromatics is presented in Figure 7. Increasing LHSV has a negative effect on the elimination of sulfur and aromatics, because increasing LHSV causes the residence time to decrease, and consequently the reactions could not proceed enough.

Figure 8 illustrates the effect of H_2/oil ratio on the outlet concentrations of sulfur and aromatics. Increasing the H_2/oil ratio has a positive effect on reducing the sulfur and aromatics, because the inlet flow of hydrogen is a direct function of this ratio.

4.4. Optimization Results. Optimization was considered for a TBR for diesel HT. NSGA II was used to optimize and obtain Pareto-optimal solutions. A Pareto-optimal set is a series of solutions that are non-dominated with respect to each other. When moving from one Pareto solution to another, there is always a certain amount of sacrifice in one objective(s) to achieve a certain amount of gain in other(s). Figure 9 shows an example of a Pareto-optimal set (Pareto frontier). The points represent feasible choices, and smaller values are preferred to larger ones. Point C is not on the Pareto frontier because it is dominated by both point A and point B. Points A and B are not strictly dominated by any other $(f_1(A) > f_1(B), f_2(A) < f_2(B))$, and hence they do lie on the frontier.

There were two objectives of the optimization:

(I) minimizing the sulfur concentration in the liquid phase at the end of the reactor

(II) minimizing the aromatics concentration in the liquid phase at the end of the reactor

subject to[3]

$$330\ ^\circ\text{C} \le \text{feed temperature} \le 400\ ^\circ\text{C}$$

$$4\ \text{MPa} \le \text{reactor pressure} \le 7\ \text{MPa}$$

$$1\ h^{-1}(8.75 \times 10^{-3}\ \text{cm/s}) \le \text{LHSV} \le 2\ h^{-1}(1.75 \times 10^{-2}\ \text{cm/s})$$

$$60 \le H_2/\text{oil} \le 400$$

$$0 \le \text{initial partial pressure of } H_2S \le 3.5 \times 10^{-3}\ \text{MPa}$$

Other parameters were the same as in the base case.

Different operations were performed for 200 generations to obtain non-dominated Pareto-optimal solutions. A population size of 50 was chosen with the crossover of 0.7 and mutation probability of 0.05. Input parameters of NSGA II are given in Table 5.

The Pareto-optimal solution sets after 200 generations are shown in Table 6 and Figure 10.

It can be seen that the optimum parameters were determined for minimum sulfur and aromatics concentrations in the liquid phase at the end of the reactor. Table 6 shows that optimized sulfur and aromatics concentrations in the liquid phase at the end of the reactor are almost zero. This table shows that each of the solutions is better than the others in at least one of the objective functions. Thus, the user has to decide among them on the basis of the ease of operation, experience, cost involved,

DOI: 10.1021/acs.energyfuels.5b00467
Energy Fuels 2015, 29, 3041−3051

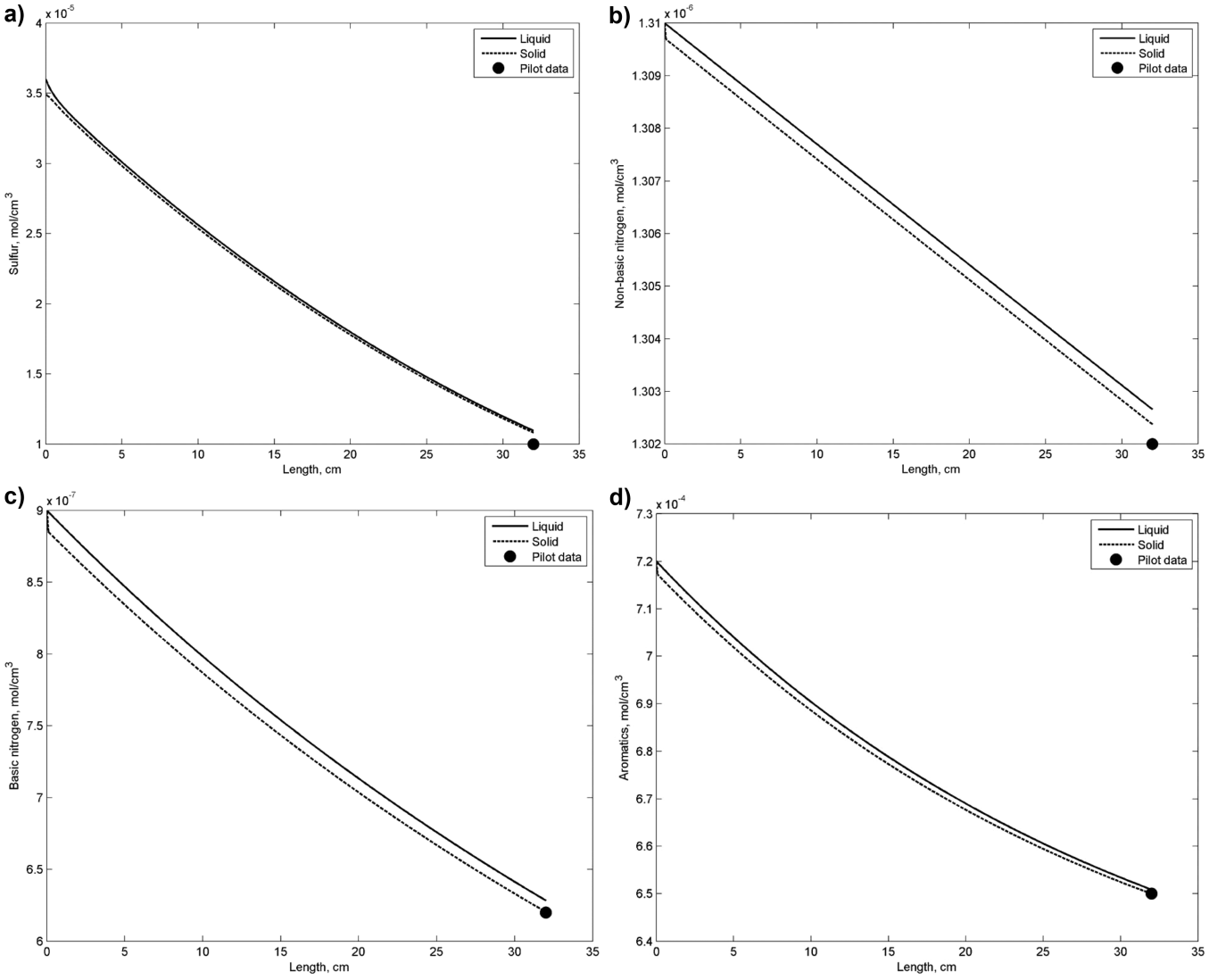

Figure 4. Comparison between simulated concentration profiles for (a) sulfur, (b) non-basic nitrogen, (c) basic nitrogen, and (d) aromatics with pilot-plant experimental data from the literature.[17]

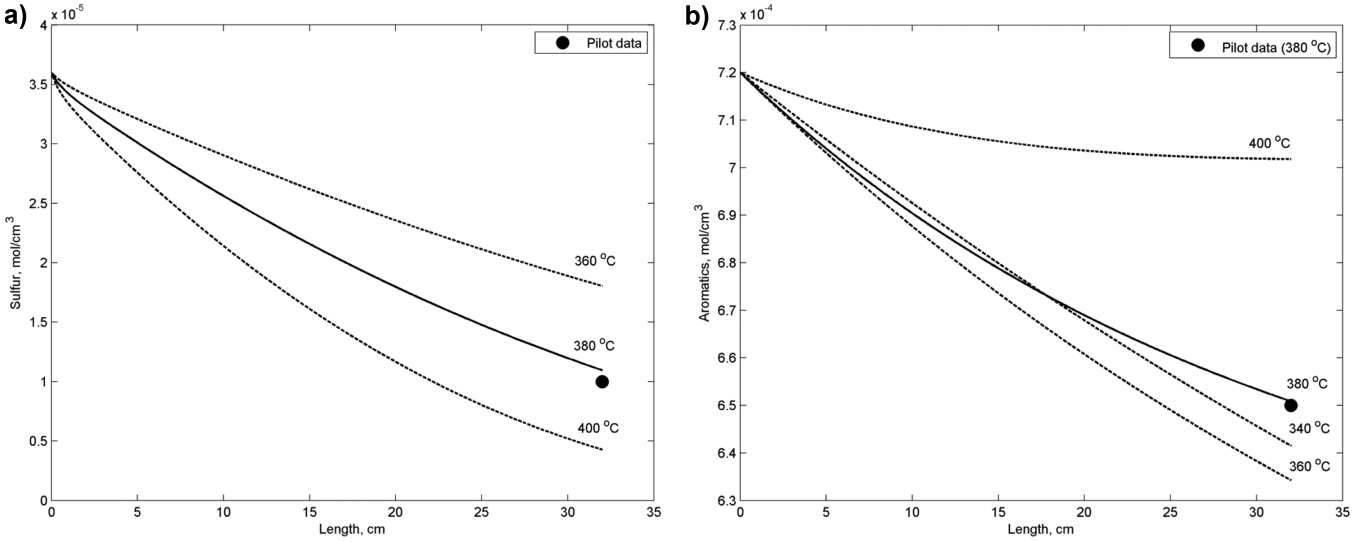

Figure 5. Effect of temperature on (a) sulfur and (b) aromatics concentration profiles in the HT reactor.

DOI: 10.1021/acs.energyfuels.5b00467
Energy Fuels 2015, 29, 3041−3051

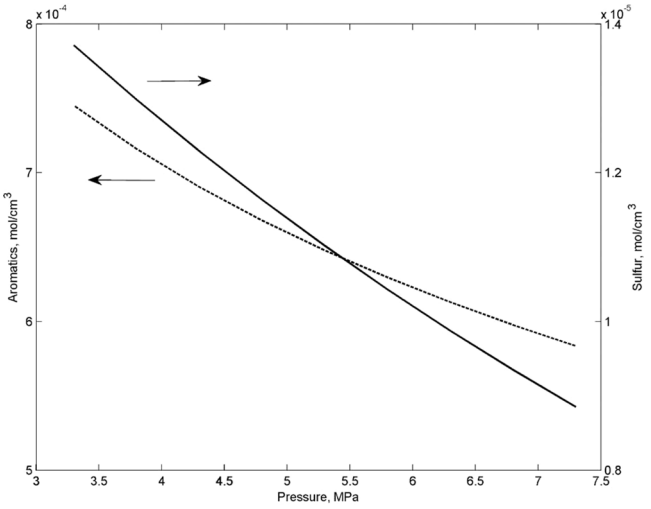

Figure 6. Effect of pressure on outlet concentrations of sulfur and aromatics in the HT reactor.

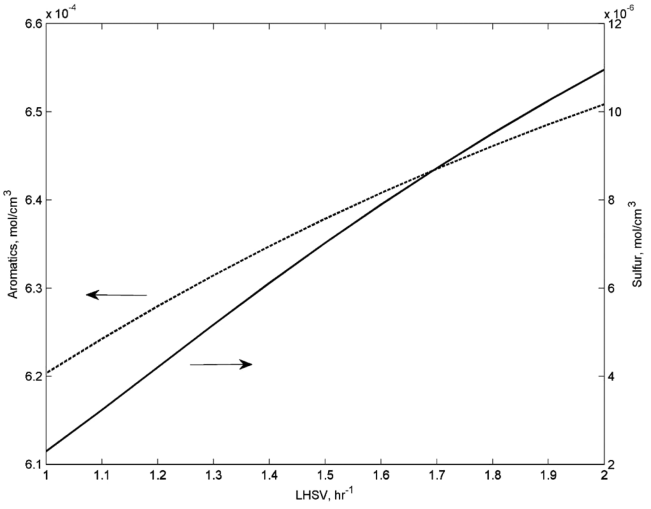

Figure 7. Effect of LHSV on outlet concentrations of sulfur and aromatics in the HT reactor.

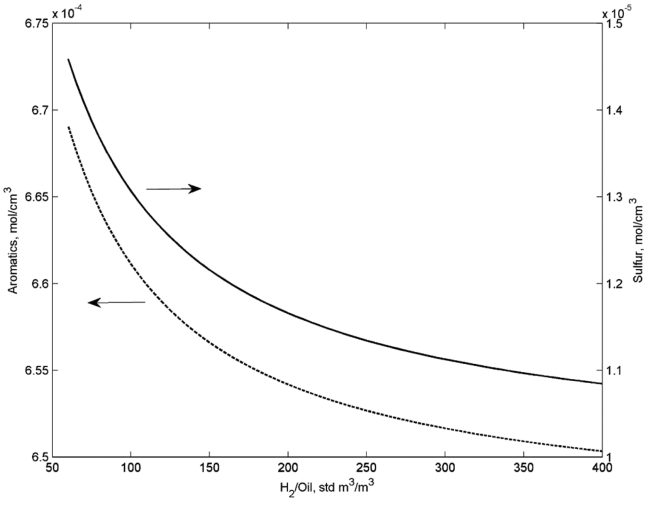

Figure 8. Effect of H_2/oil ratio on outlet concentrations of sulfur and aromatics in the HT reactor.

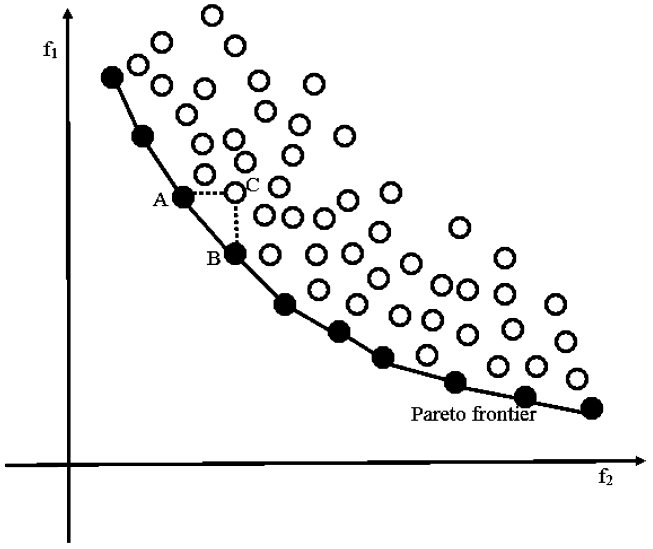

Figure 9. Example of a Pareto-optimal solution set.

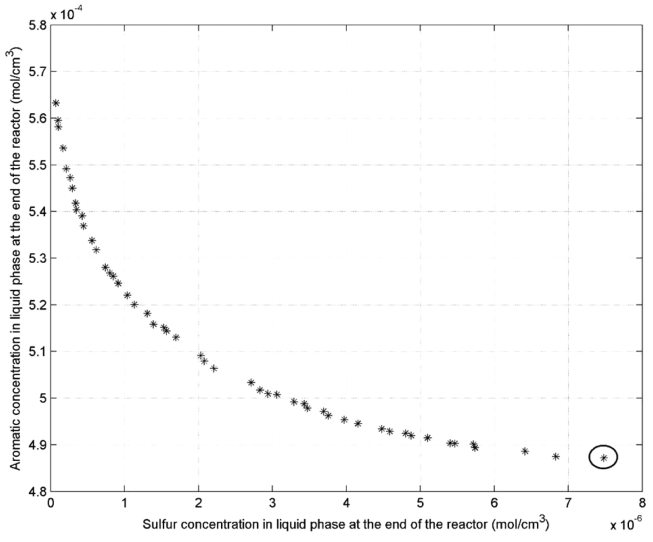

Figure 10. Pareto-optimal solution set after 200 generations.

and also the quality of the product. The optimum adjustment parameters are determined to be the following: feed temperature, 364−400 °C; reactor pressure, 7 MPa; LHSV, 1 h^{-1}; H_2/oil ratio, 355−393; and initial partial pressure of H_2S, 0.00111−0.00201 MPa.

The objective functions and reactor pressure were approximately equal in all the optimum solutions (given in Table 6). In chromosome 2, feed temperature was the lowest of all the chromosomes. Very high inlet gas temperatures are not recommended for economic reasons and because they produce high catalyst temperatures, and thus catalyst deactivation due to coke formation and even catalyst destruction by sintering. Therefore, chromosome 2 can be considered the most appropriate solution for the diesel HT process (given in Table 6). This chromosome was also specified in Figure 10.

5. CONCLUSIONS

The objective of this work was to use a one-dimensional heterogeneous model with three main reactions—HDS, HDN, and HDA—to simulate a diesel HT reactor. The model results show good agreement with the experimental data. The effects

DOI: 10.1021/acs.energyfuels.5b00467
Energy Fuels 2015, 29, 3041−3051

Table 6. Pareto-Optimal Solution Set after 200 Generations

no.	feed temp (°C)	reactor pressure (MPa)	liquid space velocity (cm s^{-1})	H_2/oil ratio	initial partial pressure of H_2S (MPa)	concn in liquid phase at end of reactor (mol cm^{-3}) sulfur	aromatics
1	400	7.0000	0.00875	370	0.00111	7.10×10^{-8}	0.000563
2	364	7.0000	0.00879	365	0.00194	7.48×10^{-6}	0.000487
3	367	7.0000	0.00879	359	0.00201	6.42×10^{-6}	0.000489
4	366	6.9987	0.00877	372	0.00156	6.83×10^{-6}	0.000487
5	381	6.9841	0.00876	393	0.00169	2.21×10^{-6}	0.000506
6	379	6.9940	0.00877	364	0.00191	2.71×10^{-6}	0.000503
7	397	6.9968	0.00878	355	0.00157	1.70×10^{-7}	0.000554
8	383	6.9876	0.00876	366	0.00181	1.70×10^{-6}	0.000513
9	382	6.9884	0.00876	368	0.00133	2.03×10^{-6}	0.000509
10	369	7.0000	0.00876	364	0.00163	5.74×10^{-6}	0.000489
11	391	6.9998	0.00878	365	0.00172	6.18×10^{-7}	0.000532
12	396	6.9805	0.00878	378	0.00166	2.12×10^{-7}	0.000549
13	374	6.9990	0.00876	366	0.00177	4.16×10^{-6}	0.000495
14	371	6.9951	0.00878	368	0.00171	5.10×10^{-6}	0.000491
15	391	6.9959	0.00878	364	0.00160	5.60×10^{-7}	0.000534
16	386	6.9917	0.00877	364	0.00149	1.31×10^{-6}	0.000518
17	389	7.0000	0.00875	366	0.00188	7.40×10^{-7}	0.000528
18	387	6.9957	0.00876	367	0.00165	1.04×10^{-6}	0.000522
19	392	6.9989	0.00876	367	0.00156	4.44×10^{-7}	0.000537
20	399	6.9998	0.00875	369	0.00112	1.06×10^{-7}	0.000558
21	387	6.9975	0.00876	369	0.00143	1.13×10^{-6}	0.000520
22	395	6.9987	0.00878	357	0.00181	2.94×10^{-7}	0.000545
23	373	6.9992	0.00878	365	0.00180	4.48×10^{-6}	0.000493
24	388	6.9938	0.00877	368	0.00171	9.15×10^{-7}	0.000525
25	375	6.9990	0.00876	366	0.00177	3.97×10^{-6}	0.000495
26	377	6.9969	0.00877	364	0.00194	3.29×10^{-6}	0.000499
27	399	6.9995	0.00875	363	0.00128	1.00×10^{-7}	0.000560
28	385	6.9998	0.00875	369	0.00174	1.39×10^{-6}	0.000516
29	378	6.9949	0.00877	364	0.00167	3.06×10^{-6}	0.000501
30	394	7.0000	0.00876	362	0.00186	3.40×10^{-7}	0.000542
31	370	6.9976	0.00876	364	0.00173	5.40×10^{-6}	0.000490
32	395	6.9656	0.00875	368	0.00176	2.66×10^{-7}	0.000547
33	378	6.9981	0.00875	369	0.00170	2.83×10^{-6}	0.000502
34	375	7.0000	0.00876	366	0.00178	3.76×10^{-6}	0.000496
35	382	6.9974	0.00875	371	0.00169	2.08×10^{-6}	0.000508
36	375	6.9944	0.00876	364	0.00200	3.69×10^{-6}	0.000497
37	393	6.9878	0.00878	361	0.00145	4.28×10^{-7}	0.000539
38	376	6.9996	0.00876	365	0.00175	3.48×10^{-6}	0.000498
39	373	6.9988	0.00876	364	0.00164	4.59×10^{-6}	0.000493
40	372	7.0000	0.00878	364	0.00166	4.88×10^{-6}	0.000492
41	372	6.9986	0.00878	363	0.00174	4.80×10^{-6}	0.000492
42	384	6.9905	0.00877	368	0.00150	1.57×10^{-6}	0.000514
43	369	6.9964	0.00879	361	0.00179	5.72×10^{-6}	0.000490
44	393	6.9989	0.00875	370	0.00135	3.50×10^{-7}	0.000540
45	370	7.0000	0.00878	366	0.00182	5.47×10^{-6}	0.000490
46	378	6.9983	0.00875	369	0.00167	2.94×10^{-6}	0.000501
47	389	6.9909	0.00876	367	0.00172	8.48×10^{-7}	0.000526
48	376	6.9880	0.00876	366	0.00169	3.43×10^{-6}	0.000499
49	384	6.9741	0.00880	388	0.00178	1.54×10^{-6}	0.000515
50	389	6.9946	0.00876	370	0.00170	8.00×10^{-7}	0.000527

of important operating parameters such as temperature, pressure, LHSV, and H_2/oil ratio on HDS, HDN, and HDA reactions were considered.

Increasing temperature has a positive effect on HDS and HDN reactions, but for HDA, the outlet concentration reduces with increasing temperature until 360 °C, above which the concentration increases due to the reversibility of this saturation reaction. Higher pressure and H_2/oil ratio reduce the outlet concentrations of sulfur and aromatics. However, increasing LHSV has a negative effect on all of the reactions.

Finally, NSGA II was used to optimize and obtain Pareto-optimal solutions. The objectives were to obtain minimal concentrations of sulfur and aromatics in the liquid phase at the end of the reactor. The adjustable parameters were feed

DOI: 10.1021/acs.energyfuels.5b00467
Energy Fuels 2015, 29, 3041−3051

temperature, reactor pressure, LHSV, H_2/oil ratio, and initial partial pressure of H_2S. The results show that the optimized sulfur and aromatic concentrations in the liquid phase at the end of the reactor are almost zero with the parameters adjusted to 364−400 °C, 7 MPa, 1 h^{-1}, 355−393, and 0.00111−0.00201 for feed temperature, reactor pressure, LHSV, H_2/oil ratio, and initial partial pressure of H_2S, respectively.

AUTHOR INFORMATION

Corresponding Author

*E-mail: alebrm@aut.ac.ir.

Notes

The authors declare no competing financial interest.

NOMENCLATURE

HT = hydrotreating
HDS = hydro-desulfurization
HDN = hydro-denitrogenation
HDA = hydro-dearomatization
TBR = trickle-bed reactor
VGO = vacuum gas oil
LHSV = liquid hourly space velocity (h^{-1})
API = American Petroleum Institute (API) gravity
S = sulfur
A = aromatic compound
N_B = basic nitrogen
N_{NB} = non-basic nitrogen
Np = naphthenes
z = reactor length (cm)
R_p = radius of catalyst pellet (cm)
r = radius of catalyst (cm)
d_p = particle diameter (cm)
a_L = gas−liquid interfacial area (cm^{-1})
a_s = liquid−solid interfacial area (cm^{-1})
C_i = molar concentration of compound i (mol cm^{-3})
D_i^L = molecular diffusivity of compound i in liquid (cm^2 s^{-1})
E_a = activation energy (J mol^{-1})
T_{MeABP} = mean average boiling point (°R)
G_L = liquid superficial mass velocity (g cm^{-2} s^{-1})
k_f = forward HDA rate constant (s^{-1} MPa^{-1})
k_r = reverse HDA rate constant (s^{-1})
k_j = reaction rate constant for reaction$j$ (see Table 1)
k_i^j = mass-transfer coefficient of compound i at the interface j (cm s^{-1})
H_i = Henry's law coefficient, MPa·cm^3 mol^{-1}
K_{H_2S} = adsorption equilibrium constant for H_2S (cm^3 mol^{-1})
p_i^j = partial pressure of compound i in the j phase (MPa)
r_j = reaction rate j
R = universal gas constant (J mol^{-1} K^{-1})
T = temperature (K)
u_j = superficial velocity of j phase (cm s^{-1})

Greek Symbols

η_j = catalyst effectiveness factor for reaction j
ρ_B = catalyst bulk density
λ_i = solubility coefficient of compound i (Nl kg^{-1} MPa^{-1})
ρ_0 = liquid density at standard conditions (15.6 °C and 101.3 kPa) (lb ft^{-3})
ρ_{20} = liquid density at 20 °C (g cm^{-3})
μ_L = liquid viscosity (mPa·S)
ν_c = critical specific volume of the gaseous compounds (cm^3 mol^{-1})
ν_i = molar volume of the solute i at normal boiling temperature (cm^3 mol^{-1})
ν_L = molar volume of solvent liquid at normal boiling temperature (cm^3 mol^{-1})
ν_N = molar gas volume at standard conditions (Nl mol^{-1})
ν_c^m = critical specific volume (ft^3 lb_m^{-1})

Subscripts

j = reaction (HDS, HDN_B, HDN_{NB}, or HDA)
G = gas phase
L = liquid phase
0 = reactor inlet condition

Superscripts

G = gas phase
L = liquid phase
s = solid phase

REFERENCES

(1) European standards for gasoline and for diesel: European Standards Organization (CEN), EN 228:1999 for gasoline, and EN 590:2004 for diesel fuel.
(2) Gary, J. H.; Handwerk, G. E. *Petroleum Refining*; Marcel Dekker: New York, 2001.
(3) Fahim, M. A.; Al-Sahhaf, T. A.; Elkilani, A. S. *Fundamentals of Petroleum Refining*; Elsevier: Oxford, 2010.
(4) Ancheyta, J. *Modeling and Simulation of Catalytic Reactors for Petroleum Refining*; John Wiley & Sons: New York, 2011.
(5) Korsten, H.; Hoffmann, U. Three-Phase Reactor Model for Hydrotreating in Pilot Trickle-Bed Reactors. *AIChE J.* **1996**, *42*, 1350−1360.
(6) Bhaskar, M.; Valavarasu, G.; Sairam, B.; Balaraman, K. S.; Balu, K. Three-Phase Reactor Model to Simulate the Performance of Pilot-Plant and Industrial Trickle-Bed Reactors Sustaining Hydrotreating Reactions. *Ind. Eng. Chem. Res.* **2004**, *43*, 6654−6669.
(7) Mejdell, T.; Myrstad, R.; Morud, J.; Rosvoll, J. S.; Steiner, P.; Blekkan, E. A. A new kinetic model for hydrodesulfurization of oil products. *Stud. Surf. Sci. Catal.* **2001**, *133*, 189−194.
(8) Lopez, R.; Dassori, C. G. Mathematical Modeling of a VGO Hydrotreating Reactor, SPE-69499; Presented at the SPE Latin American and Caribbean Petroleum Engineering Conference, March 25−28, 2001, Buenos Aires, Argentina; Society of Petroleum Engineers: Richardson, TX, 2001.
(9) Avaraam, D. G.; Vasalos, I. A. HdPro: A Mathematical Model of Trickle-Bed Reactors for the Catalytic Hydroprocessing of Oil Feedstocks. *Catal. Today* **2003**, *79−80*, 275−283.
(10) Rodriguez, M. A.; Ancheyta, J. Modeling of Hydrodesulfurization (HDS), Hydrodenitrogenation (HDN), and the Hydrogenation of Aromatics (HDA) in a Vacuum Gas Oil Hydrotreater. *Energy Fuels* **2004**, *18*, 789−794.
(11) Jimenz, F.; Kafarov, V.; Nunez, M. Modeling of Industrial Reactor for Hydrotreating of Vacuum Gas Oils Simultaneous Hydrodesulfurization, Hydrodenitrogenation and HydrodearomatizationReactions. *Chem. Eng. J.* **2007**, *134*, 200−208.
(12) Melis, S.; Lara, E.; Sassu, L.; Baratti, R. A model for the hydrogenation of aromatic compounds during gasoil hydroprocessing. *Chem. Eng. Sci.* **2004**, *59*, 5671−5677.
(13) Macias, M. J.; Ancheyta, J. Simulation of an isothermal hydrodesulfurization small reactor with different catalyst particle shapes. *Catal. Today* **2004**, *98*, 243−252.
(14) Cheng, Z.-M.; Fang, X.-C.; Zeng, R.-H.; Han, B.-P.; Huang, L.; Yuan, W.-K. Deep removal of sulfur and aromatics from diesel through tw-stage concurrently and countercurrently operated fixed-bed reactors. *Chem. Eng. Sci.* **2004**, *59*, 5465−5472.
(15) Mederos, F. S.; Ancheyta, J.; Elizade, I. Dynamic Modeling and Simulation of Hydrotreating of Gas Oil Obtained from Heavy Crude Oil. *Appl. Catal. A: General* **2012**, *425−426*, 13−27.

DOI: 10.1021/acs.energyfuels.5b00467
Energy Fuels 2015, 29, 3041−3051

(16) Jarullah, A. T.; Mujtaba, I. M.; Wood, A. S. Improving fuel quality by whole crude oil hydrotreating: A kinetic model for hydrodeasphaltenization. *Appl. Energy* **2012**, *94*, 182−191.
(17) Mederos, F. S.; Rodriguez, M. A.; Ancheyta, J.; Arce, E. Dynamic Modeling and Simulation of Catalytic Hydrotreating Reactors. *Energy Fuels* **2006**, *20*, 936−945.
(18) Yui, S. M.; Sanford, C. Kinetics of Aromatics Hydrogenation of Bitumen-Derived Gas Oils. *Can. J. Chem. Eng.* **1991**, *69*, 1087−1095.
(19) Roberts, G. W. *Chemical Reactions and Chemical Reactors*; John Wiley & Sons: New York, 2009.
(20) Froment, G. F.; Bischoff, K. B.; De Wilde, J. *Chemical Reactor Analysis and Design*, 3rd ed.; John Wiley & Sons: New York, 2011.
(21) Azarhoosh, M. J.; Farivar, F.; Ale Ebrahim, H. Simulation and Optimization of a Horizontal Ammonia Synthesis Reactor using Genetic Algorithm. *RSC Adv.* **2014**, *4*, 13419−13429.
(22) Shopova, E. G.; Vaklieva-Bancheva, N. G. Basic Genetic Algorithm for Engineering Problem Solutions. *Comput. Chem. Eng.* **2006**, *30*, 1293−1309.
(23) Azarhoosh, M. J.; Ale Ebrahim, H.; Pourtarah, S. H. Simulating and Optimizing Auto-Thermal Reforming of Methane to Synthesis Gas Using Non-Dominated Sorting Genetic Algorithm II Method. *Chem. Eng. Commun.* **2014**, DOI: 10.1080/00986445.2014.942732.
(24) Suli, E.; Mayers, D. *An Introduction to Numerical Analysis*; Cambridge University Press: Cambridge, UK, 2003.
(25) Behroozsarand, A.; Ebrahimi, H.; Zamaniyan, A. Multiobjective Optimization of Industrial Autothermal Reformer for Syngas Production Using Nonsorting Genetic Algorithm II. *Ind. Eng. Chem. Res.* **2009**, *48*, 7529−7539.

DOI: 10.1021/acs.energyfuels.5b00467
Energy Fuels 2015, 29, 3041−3051